

pubs.acs.org/ac Article

Antibody-Directed Cell Internalization of Targeted Covalent Europium Tag Enables In Situ Kinase Labeling and Inductively Coupled Plasma Mass Spectrometry (ICP-MS) Quantification

Ziyang Fang,[§] Xinyue Zhao,[§] Ruxue Hou,[§] Yang Zhao, Lei Wang, Li Yi, Limin Yang, Xiaowen Yan,^{*} and Qiuquan Wang



Cite This: Anal. Chem. 2025, 97, 12125–12132



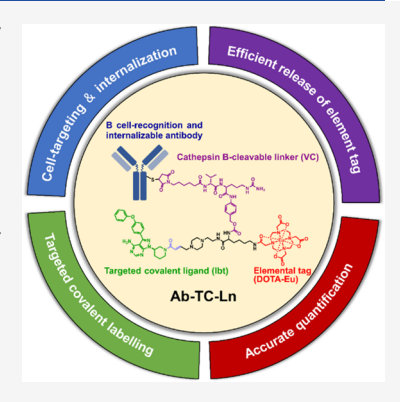
ACCESS I

III Metrics & More

Article Recommendations

Supporting Information

ABSTRACT: Development of methods to accurately detect the expression and activity of protein targets inside live cells is of great significance for disease diagnostics and drug development. Inductively coupled plasma mass spectrometry (ICP-MS) has been demonstrated as a promising technology for protein quantification, the key of which is developing element tags to selectively label the specific protein targets in complex samples with elements sensitive in ICP-MS. Numerous small-molecule element tags (SM-ETs) using DOTA as a lanthanide (Ln) chelating agent have been developed for specific protein target labeling. However, the existing DOTA-based SM-ETs still face limitations including the lack of cell targeting property and low cellular uptake as a result of the inability to penetrate the cell membrane for direct intracellular protein labeling, which restricts the application of SM-ETs for in situ protein quantification. Herein, we present a novel antibody-directed cell/protein dual-targeting strategy that enables us to specifically label and quantify protein targets inside live cells. Based on this strategy, we constructed a multifunctional antibody-targeted covalent



Ln tag (Ab-TC-Ln, LTX-VC-Ibt-DOTA-Eu), comprising a cell-permeable monoclonal antibody (Loncastuximab, LTX), a targeted covalent Ln tag (Ibt-DOTA-Eu) for Bruton's tyrosine kinase (BTK), and between them a cathepsin B-cleavable linker (VC). LTX-TC-Ln enables cancer cell recognition, internalization, release of targeted covalent element tags, and specific labeling of Ln to intracellular BTK for ICP-MS quantification. Our work establishes a promising antibody-directed cell internalization strategy for intracellular protein Ln labeling and quantification, which will inspire the development of new ICP-MS approaches toward the quantification of other important protein targets in the future.

INTRODUCTION

Inductively coupled plasma mass spectrometry (ICP-MS)¹ has been recognized as a powerful tool for the quantification of antigens,² proteases,^{3,4} and cells.^{5,6} In order to convert the quantification of biomolecules into the quantification of metal elements by ICP-MS, it is crucial to selectively label metal atoms onto targeted biomolecules. Therefore, great efforts have been put into developing element tags (ETs) with high sensitivity and selectivity, which normally consist of a metal moiety as the signal reporter of ICP-MS and a targeting group for biomolecule recognition and labeling. Considering the benefits of minimal polyatomic interference, low background interference, ionization efficiency of up to 100% in argon plasma, and detection limits down to pg/L in ICP-MS, lanthanides (Ln) are especially suitable for ICP-MS-based protein quantification. 1-3,5-13 1,4,7,10-Tetraazacyclododecane-1,4,7,10-tetraacetic acid (DOTA), which can form extremely stable complexes with Ln, is widely used as the macrocyclic chelating agent for developing element tags. 13,14 Based on the type of targeting group used, the numerous Ln tags that have been developed can be mainly divided into two

categories: antibody element tags (Ab-ETs)^{1,2,5-10,14} and small-molecule element tags (SM-ETs).^{3,11,13,15,16}

Thanks to the high selectivity of antibody to antigen, Ab-ETs have been successfully applied for multiparametric analysis of biomarkers, whether in a free state 1,7,8 or bound on the cell surface. 5,6,9,10,14 However, the precise number of Ln atoms labeled on an antibody is usually uncertain. In addition, antibody and antigen bind through noncovalent interactions, leading to an ambiguous labeling ratio. As a result, the stoichiometric ratio between Ln atoms and the targeted antigen labeled by Ab-ETs is difficult to control for precise quantification.

In terms of SM-ETs, accurate labeling of a defined number of Ln atoms to a targeted biomolecule has been achieved,

Received: January 22, 2025 Revised: May 10, 2025 Accepted: May 30, 2025 Published: June 5, 2025





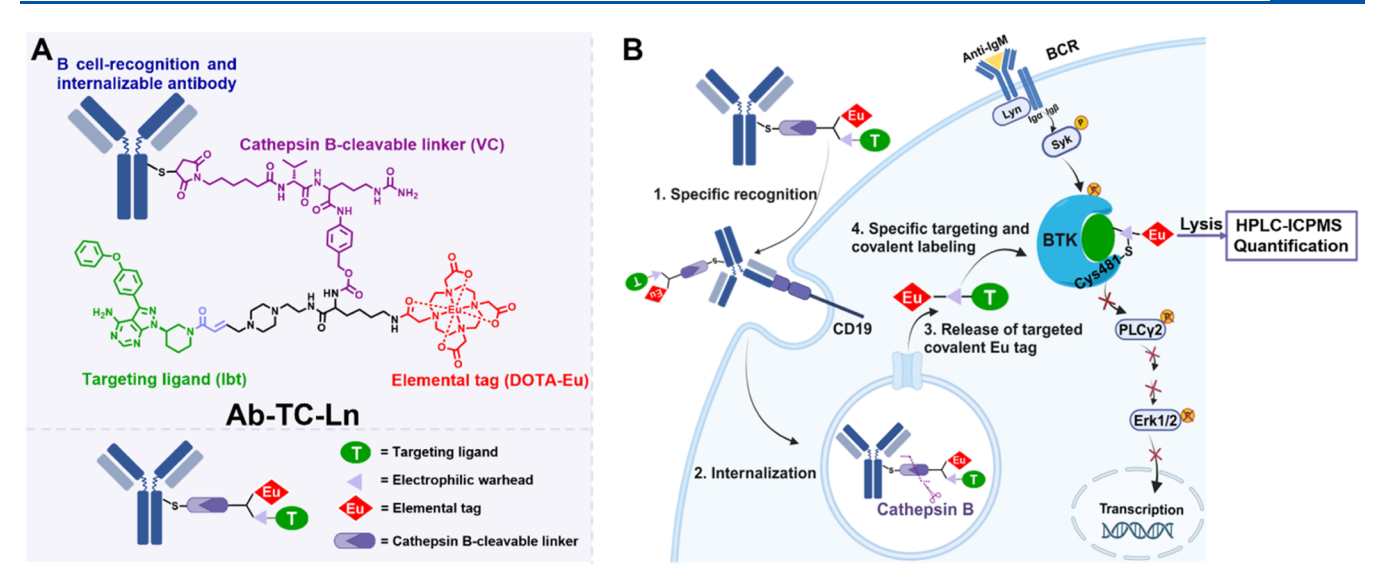


Figure 1. (A) Design of the multifunctional antibody-targeted covalent lanthanide tag (Ab-TC-Ln, LTX-VC-Ibt-DOTA-Eu). (B) Mechanism of multifunctional Ab-TC-Ln for cell recognition, internalization, and in situ BTK labeling and quantification.

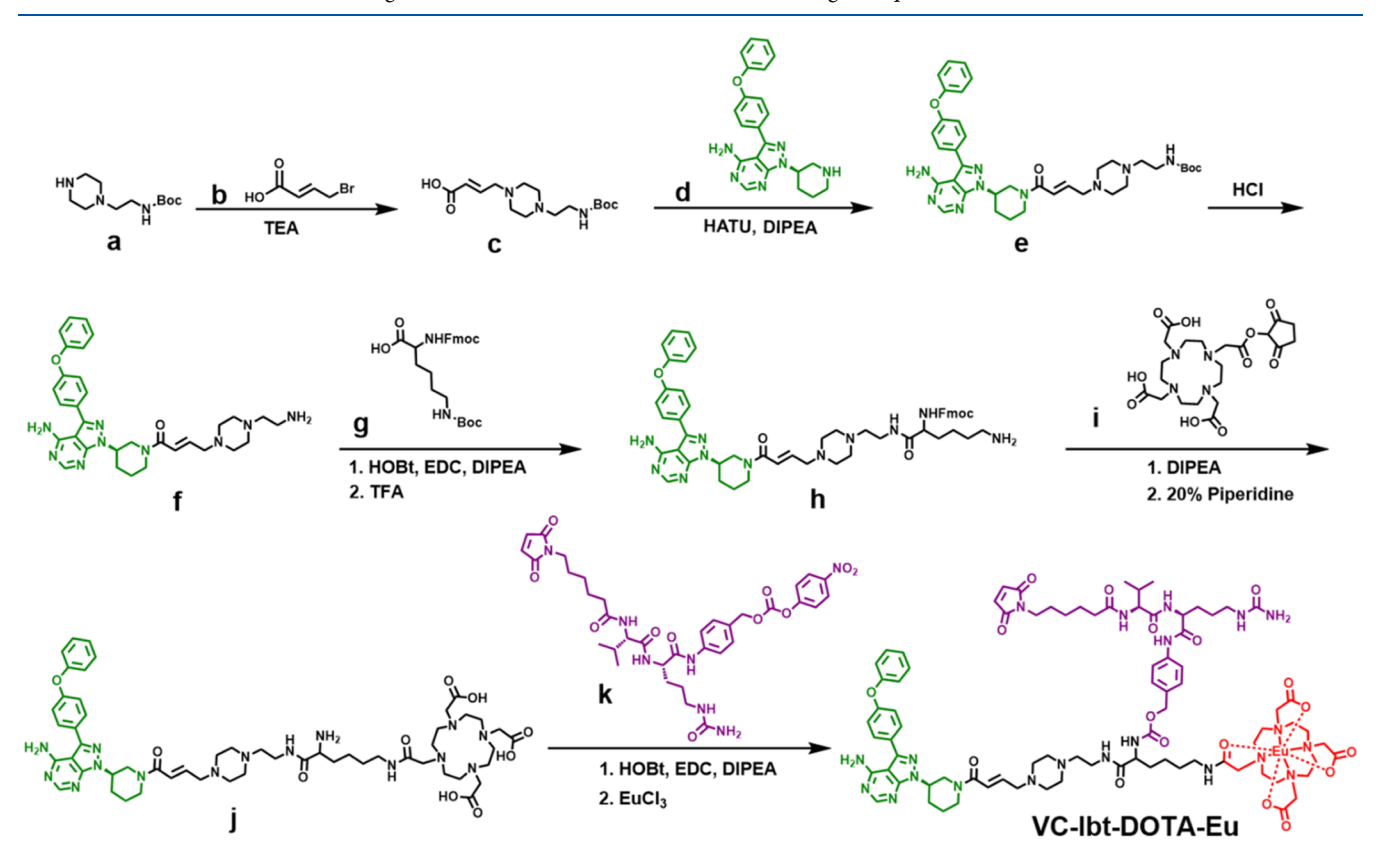


Figure 2. Synthetic route of VC-Ibt-DOTA-Eu.

because the number of Ln atom on each SM-ET can be precisely controlled, and the labeling stoichiometry of SM-ET to the targeted biomolecule, such as proteases^{3,16} or kinases,^{11,15} has been realized by using irreversible enzyme inhibitors or targeted covalent inhibitors as the specific targeting groups. Furthermore, based on the unique property that the signal of an element is independent of its chemical form, i.e., either in a free state or tagged on a protein, the SM-ET-labeled proteins can be absolutely quantified by species-unspecific isotope dilution (SUID) ICP-MS using only one element/isotope standard. A series of chemically selective and

biologically specific SM-ET labeling strategies have been developed for absolute quantification of different biomolecules using HPLC/SUID-ICP-MS.^{3,11,13,17,18} However, the existing SM-ETs still face some limitations that hamper their real application. For example, although some SM-ETs show high selectivity to protein targets, they lack the ability to recognize a specific cell simultaneously. Furthermore, the SM-ETs using DOTA-Ln as the signal reporter have been recently found to be unable to penetrate the cell membrane for direct intracellular protein labeling and quantification, ¹¹ restricting

the direct application of SM-ETs for in situ protein quantification.

In this study, we aim to develop a strategy enabling the targeted delivery and internalization of SM-ETs to live cancer cells and further tagging Ln to a specific intracellular protein for ICP-MS quantification. To this end, we propose a novel antibody-directed cell and protein dual-targeting strategy for in situ protein labeling and quantification through developing a multifunctional antibody-targeted covalent Ln tag (Ab-TC-Ln). Ab-TC-Ln consists of a cell internalizable monoclonal antibody, a DOTA-Ln-modified targeted covalent tag (TC-Ln) and, between them, a cleavable linker. The Ab-TC-Ln enables (1) recognition of target cells with high specificity; (2) penetration of the cell membrane with high internalization efficiency; (3) rapid release of Ln tag; (4) specific labeling of intracellular protein target with a stoichiometry number of Ln.

Herein, we selected Bruton's tyrosine kinase (BTK),¹⁹ a key component of the B-cell receptor (BCR) signaling pathway crucial for the survival and proliferation of B-cell malignancies,²⁰ as the model protein target. Ibrutinib (Ibt),²¹ a TC inhibitor of BTK approved by the FDA for B-cell malignancies, is selected as the TC ligand of TC-Ln. Meanwhile, we selected loncastuximab (LTX),²² a cell internalizable monoclonal antibody that can specifically recognize CD19 receptor present on the surface of B-cell lymphoma cells, to synthesize **Ab-TC-Ln**. Rituximab (RTX), an anti-CD20 antibody that cannot be internalized by cells, is used as a negative control of cell internalization.²³

Specifically, our **Ab-TC-Ln**, **LTX-VC-Ibt-DOTA-Eu**, consists of (1) a LTX as the B-cell recognition and internalization antibody; (2) a Ibt as the TC unit for BTK labeling; (3) a DOTA-Eu as the mass reporter for ICP-MS quantification; and (4) a cathepsin B-cleavable linker (Val-Cit-PABC, VC)²⁴ used to bridge Ibt-DOTA-Eu and LTX (Figure 1A).

As shown in Figure 1B, Ab-TC-Ln specifically recognizes the CD19 receptor present on the surface of B-cell lymphoma cells and is internalized into cells. Upon encountering cathepsin B inside cells, the VC linker of Ab-TC-Ln is cleaved, followed by 1,6-elimination and the release of TC-Ln (Ibt-DOTA-Eu) from the antibody. The targeting ligand of Ibt-DOTA-Eu further specifically interacts with BTK, bringing the acrylamide group in close proximity to the thiol of Cys481, resulting in the formation of a covalent bond between Ibt-DOTA-Eu and BTK. In this way, the antibody-directed cell internalization of TC-Ln and targeted covalent labeling of intracellular BTK with Ln are realized simultaneously. Furthermore, accurate detection of intracellular BTK tagged with Ln is achieved by using HPLC/SUID-ICP-MS.

■ EXPERIMENTAL SECTION

Materials and Instruments. All of the materials used can be found in the Supporting Information. The synthetic route for VC-Ibt-DOTA-Eu is summarized in Figure 2, and the details of the synthesis procedures are presented in the SI.

Synthesis and Characterization of Ab-TC-Ln. First, the interchain disulfide bond of the hinge region was reduced using TCEP. Different equivalents of TCEP were added to RTX/LTX (30 μ M) in the HEPES buffer for 2 h at 37 °C. Samples (0.5 μ g) were then heated at 95 °C for 10 min and analyzed by SDS-PAGE (100 mA, 2 h), followed by Coomassie's bright blue staining. Second, VC-Ibt-DOTA-Eu was conjugated with an antibody through the thiol-maleimide chemistry reaction, thereby obtaining an Eu-labeled antibody.

After reduction by TCEP, VC-Ibt-DOTA-Eu with different equivalents was added and reacted at 37 °C for 3 h. Then, the conjugation product was analyzed by SDS-PAGE and Coomassie's bright blue staining. The characterization of **AbTC-Ln** was performed on NanoLC-CaptiveSpray MS and MALDI-ToF MS. Chromatographic conditions: BEH C18, 0.3 μ L/min, and ACN 0 min-2% B, 8 min-2% B, 38 min-45% B, 39 min-90% B, 44 min-90% B, 45 min-2% B, and 58 min-2% B.

BTK Competitive Binding Assay. Ramos cells (5×10^6) were preincubated with increasing concentrations of Ab-TC-Ln/Ibt-DOTA-Eu for 4 h. Then, the cells were washed three times with PBS to remove excess tags. Next, the cells were incubated with probe PCI-33380 $(2 \mu M)$ for 1 h at 37 °C. After washing with the PBS buffer, cells were lysed in RIPA buffer (cat. no. R0010, Beyotime). The lysates were centrifuged at 13,000g for 10 min to remove the precipitate and further normalized by the BCA assay. Samples $(60 \mu g)$ were then heated at 95 °C for 10 min and finally resolved by SDS-PAGE and fluorescence gel scanning using a GE (AI600, USA) scanner (Ex, 460 nm; Em, Cy2 Filter).

Cell Culture and Cell Viability Assay. Ramos cells were cultured in RPMI 1640 medium with 10% fetal bovine serum. The culture dishes were maintained at 37 °C under a humid atmosphere with 5% $\rm CO_2$. Ramos cells were seeded in 96-well plates ($\rm 10^4$ cells/well) and cultured in 90 $\mu \rm L$ of medium in each well and then treated with inhibitors (0.1% DMSO) for 72 h. Ten microliters of the CCK-8 solution was added to each well and continued to culture for 1–2 h to determine the OD value at 450 nm wavelength. Each experiment was triplicated. The $\rm IC_{50}$ value was obtained by GraphPad Prism 8.0.

Confocal Fluorescence Imaging of Cells. For fluorescence imaging of live cells, Ramos cells were treated with an FITC-labeled Ab-TC-Ln (0.3 μ M) for 2, 4, 8, and 16 h, followed by washing with PBS twice before imaging. The fluorescence images of the cells were captured on the confocal laser scanning microscope ($\lambda_{\rm ex} = 488$ nm, $\lambda_{\rm em} = 516 \pm 15$ nm).

Species-Unspecific Isotope Dilution HPLC/ICP-MS (HPLC/SUID-ICP-MS). Separation of samples was carried out on a Shimadzu 20A LC system using a size exclusion chromatography column (Waters X bridge Protein BEH SEC 200 Å 3.5 μ M, 7.8 \times 300 mm). Mobile phase was used as follows: 50 mM NH₄Ac (pH 6.88) + 2% ACN; flow rate: 0.30 mL/min. The effluent from the column was mixed with the enriched ¹⁵³Eu spike solution and continuously pumped by a syringe pump (Cole-Parmer, East Bunker Court, Vernon Hills, IL) through a four-way connector. The online isotope ratio of ¹⁵³Eu to ¹⁵¹Eu was monitored using a quadrupole-based inductively coupled plasma mass spectrometer (ICP-MS) (NEXION 2000, PerkinElmer, SCIEX, Canada) equipped with a concentric pneumatic nebulizer and a cyclonic spray chamber. The ICP-MS operational parameters were as follows: nebulizer gas, 1.0 L min⁻¹; auxiliary gas, 1.2 L min⁻¹; plasma gas, 15 L min⁻¹; RF power, 1600 W; and dwell time, 100 μ s.

The online-measured ¹⁵¹Eu/¹⁵³Eu isotope chromatograms were transformed into Eu mass flow chromatograms following the isotope dilution formula shown below

$$\mathrm{MF}_{\mathrm{sample}}(t) = \mathrm{MF}_{\mathrm{spike}} \frac{M_{\mathrm{sample}}}{M_{\mathrm{spike}}} \frac{(h_{\mathrm{spike}}^{151} - h_{\mathrm{spike}}^{153} R_{\mathrm{sample}}(t))}{(h_{\mathrm{sample}}^{153} R_{\mathrm{sample}}(t) - h_{\mathrm{sample}}^{151})}$$

An online isotope dilution formula was used for transforming 151 Eu and 153 Eu isotope chromatograms into the Eu mass flow chromatogram. MF $_{\rm sample}$ and MF $_{\rm spike}$ denote the mass flow of

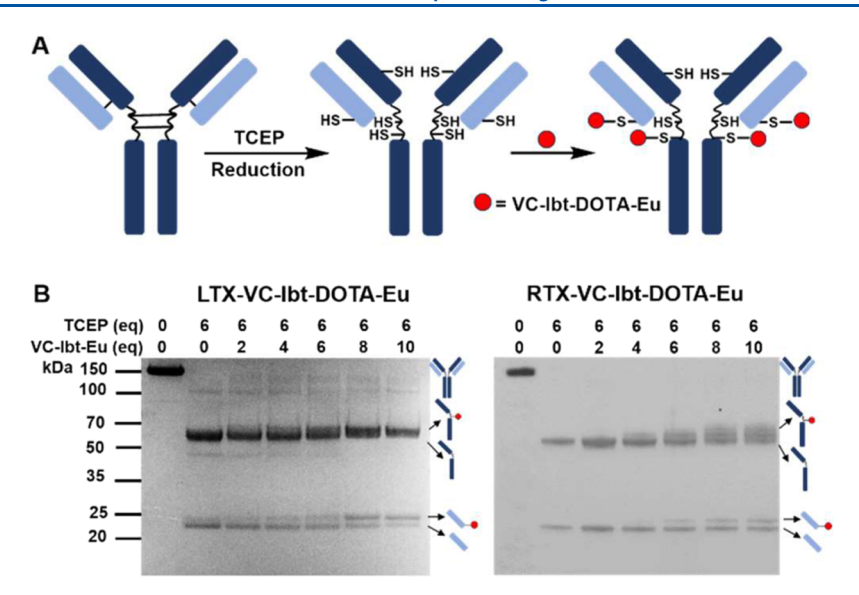


Figure 3. Synthesis and characterization of multifunctional Ab-TC-Ln. (A) Synthesis route of multifunctional Ab-TC-Ln. (B) SDS-PAGE characterization of Ab-TC-Ln prepared by labeling different equivalents of VC-Ibt-DOTA-Eu to LTX or RTX.

Eu of the sample and the spiked solution, respectively. $M_{\rm sample}$ and $M_{\rm spike}$ denote the atomic mass of Eu in the sample and the spike solution, respectively, and $h_{\rm sample}^{\rm isotope}$ and $h_{\rm spike}^{\rm isotope}$ denote the isotope abundance of the respective isotope in the sample and spike solution, respectively. $R_{\rm sample}$ (t) is the online-measured $^{151}{\rm Eu}/^{153}{\rm Eu}$ isotope ratio during HPLC/ICP-MS.

Evaluation of the Extracellular Function of Ab-TC-Ln. Separation of **Ab-TC-Ln** and Ibt-DOTA-Eu was carried out on a Shimadzu 20A LC system (Shimadzu, Japan) using a size exclusion chromatography column (Waters X bridge Protein BEH SEC 200 Å 3.5 μ M, 7.8 mm × 300 mm). An acetic amine buffer (50 mM, pH 6.8) was used as the mobile phase, and the flow rate was optimized to 0.45 mL/min. The SEC molecular weight calibration was performed with a protein standard mixture containing Loncastuximab (150 kDa), BTK (78.2 kDa), and Lysozyme (14.3 kDa). Cathepsin B (2 μ M) was added to **Ab-TC-Ln** (1 μ M) for 1 h and characterized by using SEC-ICP-MS. Ibt-DOTA-Eu (2 μ M) and BTK (0.2 μ M) were mixed for 2 h, and quantified using HPLC/SUID-ICP-MS.

Western Blot. Ramos cells $(6 \times 10^6, 2 \text{ mL})$ were treated with varying concentrations of inhibitors for 1 h, washed 3 times with PBS, and then stimulated with anti-IgM (20 μ g/mL, cat. no. SA103, Solarbio) for 10 min. The cells were lysed directly in the RIPA buffer. The lysates were cleared by centrifugation at 13,000g for 10 min at 4 °C and normalized by the BCA assay. The samples were heated at 95 °C for 10 min and analyzed by Western blot using phospho-specific antibodies Phospho-Syk (Tyr525/526, cat. no. 2710, Cell Signaling), Phospho-BTK (Tyr223, cat. no. 5082, Cell Signaling), Phospho-PLCγ2 (Tyr1217, cat. no. 3871, Cell Signaling), and Phospho-p44/42 MAPK (Erk1/2) (Thr202/Tyr204, cat. no. 4370, Cell Signaling). Chemiluminescence detection (cat. no. 35071, Thermo Fisher Scientific) was then performed. Blots were then stripped and reprobed with antibodies that specifically bound to Syk (catalog no. 2712, Cell Signaling), BTK (catalog no. 8547, Cell Signaling), PLCγ2 (catalog no. 3872, Cell Signaling), Erk (catalog no. 4695, Cell Signaling), and β -actin (catalog no. 4970, Cell Signaling) to detect the respective protein levels.

RESULTS AND DISCUSSION

Synthesis of VC-Ibt-DOTA-Eu. Figure 2 presents the synthesis route of VC-Ibt-DOTA-Eu. First, compound a reacted with compound b in the presence of TEA to obtain compound c. Compound c was then combined with compound d to afford compound e in the presence of DIPEA and HATU, followed by the acidic removal of the Boc group to obtain compound f. Compound f reacted with compound g via an amide condensation reaction to afford compound h. Compound h was then combined with compound i (DOTA), followed by Fmoc-deprotection in the presence of 20% piperidine to obtain Ibt-DOTA (compound j). Finally, VC-Ibt-DOTA-Eu was synthesized by combining Ibt-DOTA (compound j) with Val-Cit-PABC (compound k, VC), followed by chelation with Eu. Detailed synthetic steps and characterization of the above compounds are provided in the Supporting Information (Figures S1-6).

Synthesis and Characterization of Ab-TC-Ln. We prepared Ab-TC-Ln through a Michael addition reaction between the maleimide group of VC-Ibt-DOTA-Eu and the reduced interchain sulfhydryl groups of the antibody (Figure 3A). First, the interchain disulfide bond of the hinge region of the monoclonal antibody was reduced using TCEP to free the sulfhydryl group. Second, conjugation of VC-Ibt-DOTA-Eu to the monoclonal antibody via the Michael addition reaction between sulfhydryl group and maleimide to obtain multifunctional **Ab-TC-Ln** (Figure 3A). We first investigated the proper molar ratio of TCEP/LTX required for reducing the interchain disulfide bond. As shown in Figure S7, when the molar ratio of TCEP/LTX is less than 4, the interchain disulfide bond of LTX cannot be efficiently reduced, and bands of different molecular weights corresponding to different degrees of antibody reduction were observed. When the molar ratio of TCEP/LTX is ≥ 6 , the interchain disulfide bonds of LTX are efficiently reduced, and the heavy chain (H) and the light chain (L) are clearly shown on the gel. To prevent the unnecessary reduction of disulfide bonds of Ab besides the interchain disulfide bond by excess TCEP, TCEP/LTX = 6 is chosen as the ratio for reducing LTX. Second, we investigated the molar ratio of VC-Ibt-DOTA-Eu to Ab (Figure 3B). When

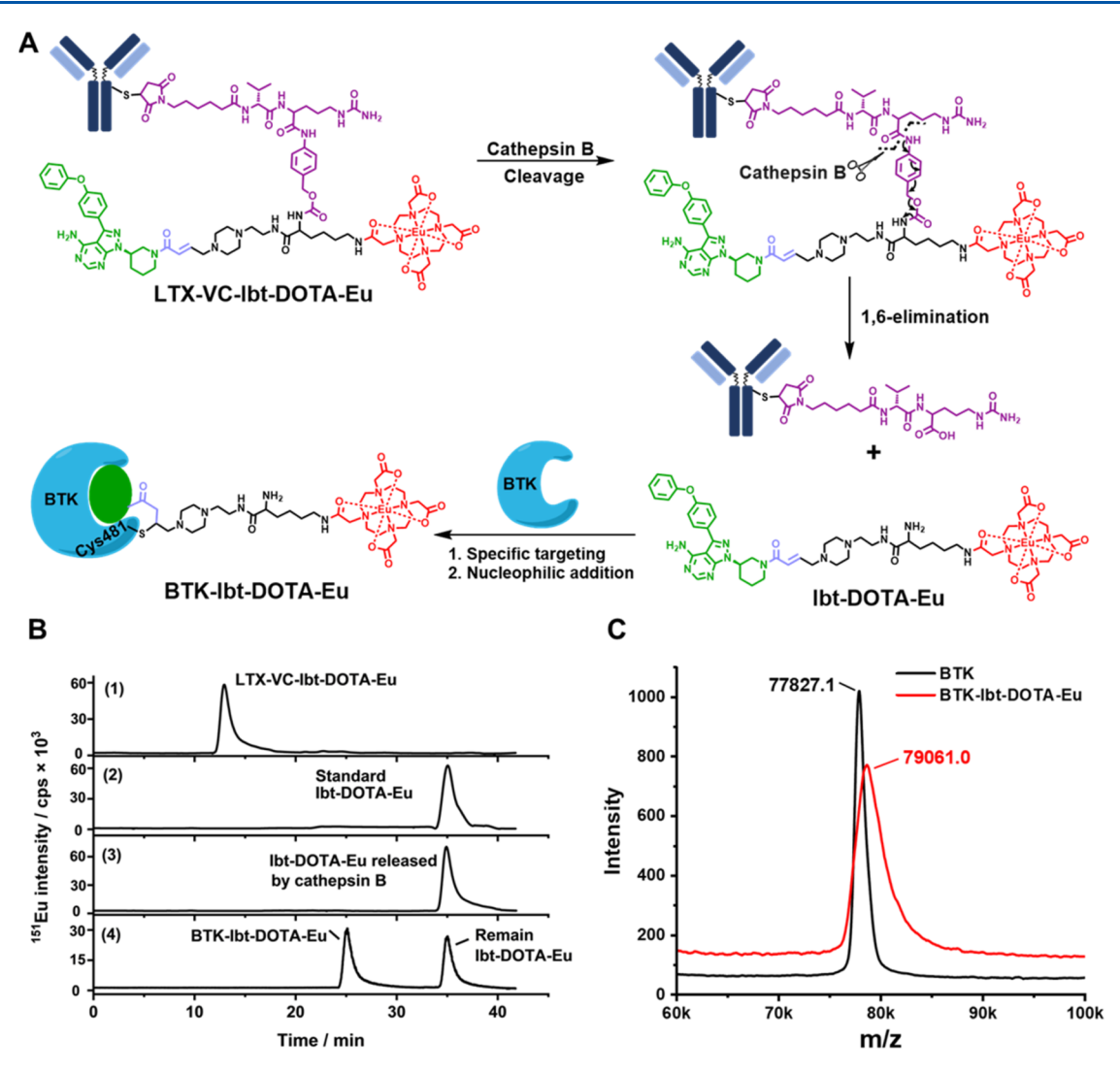


Figure 4. (A) Schematic illustrating the reaction processes of multifunctional LTX-VC-Ibt-DOTA-Eu toward cathepsin B and BTK. (B) ¹⁵¹Eu signal intensity of characterization by SEC-ICP-MS: (1) LTX-VC-Ibt-DOTA-Eu. (2) Element tag Ibt-DOTA-Eu. (3) LTX-VC-Ibt-DOTA-Eu cleavage by cathepsin B. (4) BTK labeled by Ibt-DOTA-Eu. (C) Mass spectra of Ibt-DOTA-Eu-labeled BTK as determined by MALDI-MS.

the molar ratio of VC-Ibt-DOTA-Eu to LTX is 4, there is no obvious band shift observed corresponding to the H and L chains of LTX. When the molar ratio of VC-Ibt-DOTA-Eu to LTX is ≥ 8 , an evident band shift of H and L chains is observed (Figure 3B), corresponding to the H/L-VC-Ibt-DOTA-Eu complex. We therefore chose this condition to conjugate VC-Ibt-DOTA-Eu to LTX. VC-Ibt-DOTA-Eu was successfully conjugated to RTX under the same experimental conditions (Figures 3B and S7).

We further characterized **Ab-TC-Ln** (LTX-/RTX-VC-Ibt-DOTA-Eu) using HPLC-ESI-MS, as illustrated in Figures S8–11. First, we analyzed the reduced product of LTX by the TCEP treatment (Figure S8), and the L chain of LTX was detected, supported by the deconvolution MW of 22983.8 Da. Next, the reduced LTX was treated with VC-Ibt-DOTA-Eu. As shown in Figure S9, HPLC-ESI-MS showed the conjugation of VC-Ibt-DOTA-Eu (theoretical MW = 1843.7) to the L chain of LTX (MW = 24827.6, ΔMW = 1843.7). Likewise, the L chain of RTX (MW = 23035.5) and its VC-Ibt-DOTA-Eu conjugates (MW = 24879.3, ΔMW = 1843.8) were also detected by HPLC-ESI-MS (Figures S10 and S11). However, the heavy chains of LTX and RTX were not detected through

HPLC-ESI-MS. Therefore, we further used MALDI-MS to characterize **Ab-TC-Ln**, and Figure S12 clearly shows the conjugation of VC-Ibt-DOTA-Eu to L and H chains of LTX/RTX.

Evaluation of the Extracellular Function of Ab-TC-Ln. We first investigated the extracellular response of **Ab-TC-Ln** to cathepsin B using SEC-ICP-MS. Figure 4A illustrates the reaction processes of LTX-VC-Ibt-DOTA-Eu toward cathepsin B and BTK. Upon encountering cathepsin B, the linker (VC) of LTX-VC-Ibt-DOTA-Eu is cleaved, and then Ibt-DOTA-Eu is released from the antibody as a result of the 1,6elimination reaction induced by intramolecular electron transfer. The targeting ligand of Ibt-DOTA-Eu further specifically interacts with BTK, bringing acrylamide in close proximity to the thiol of Cys481, resulting in the formation of a covalent bond between Ibt-DOTA-Eu and BTK (BTK-Ibt-DOTA-Eu). As shown in Figure 4B, upon adding cathepsin B to Ab-TC-Ln for 1 h, the peak of LTX-VC-Ibt-DOTA-Eu disappeared, and a new peak at 35.1 min was observed (Figure 4B,1,3), whose retention time was the same as that of the standard Ibt-DOTA-Eu (Figure 4B,2). The molecular weight of released Ibt-DOTA-Eu was further confirmed by HPLC-

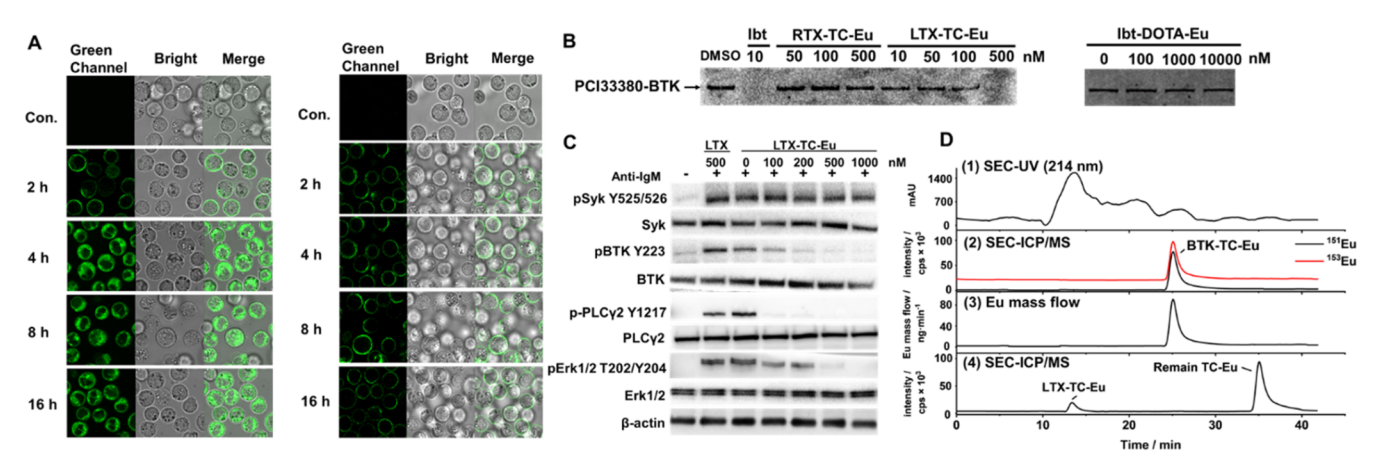


Figure 5. (A) Confocal fluorescence image of LTX-TC-Eu-FITC (left) and RTX-TC-Eu-FITC (right) in Ramos cells. (B) Concentration-dependent binding of the Ibt-DOTA-Eu released from LTX-TC-Eu-FITC/RTX-TC-Eu-FITC (left) and the free Ibt-DOTA-Eu (right) to cellular BTK in Ramos cells as determined by the competitive binding assay. (C) Concentration-dependent inhibition of BCR phosphorylation signaling in Ramos cells by LTX-TC-Eu for 24 h, as determined by SDS-PAGE immunoblotting. Blots were probed with the indicated antibodies to detect the phosphorylation of kinases along the BCR signaling pathway. (D) 1–3: SEC-ICP-MS analysis was performed to detect the reaction products of LTX-TC-Eu to cellular BTK in Ramos cells. 4: SEC-ICP-MS detected Ramos cells preincubation with ibrutinib for 1 h, followed by the addition of LTX-TC-Eu for 4 h.

ESI-MS to be the same as the standard (Figure S13). These results demonstrate that Ab-TC-Ln could be specifically cleaved by cathepsin B and release the expected Ibt-DOTA-Eu with high efficiency. Subsequently, after the co-incubation of recombinant BTK with the released Ibt-DOTA-Eu, a new peak at 25.1 min was observed (Figure 4B,4), suggesting that the released Ibt-DOTA-Eu labeled BTK to obtain BTK-Ibt-DOTA-Eu. The online-measured $^{151}\mathrm{Eu}/^{153}\mathrm{Eu}$ isotope chromatograms (Figure S14A) were transformed into a Eu mass flow chromatogram (Figure S14B) following the isotope dilution formula. By integrating the peak area and calculating based on the 1:1 reaction between BTK and Ibt-DOTA-Eu, BTK could be stably labeled with Ibt-DOTA-Eu with an 89.2 \pm 4.2% efficiency (mean \pm s.d., n = 3). As shown in Figure 4C, we further determined the MW of BTK (77827.1) and BTK-Ibt-DOTA-Eu (79061.0, Δ MW = 1233.9) using MALDI-MS, verifying a 1:1 labeling stoichiometry between BTK and Ibt-DOTA-Eu. These results demonstrate that LTX-VC-Ibt-DOTA-Eu can be specifically cleaved by cathepsin B, and released Ibt-DOTA-Eu can covalently label recombinant BTK with high efficiency.

Cell Targeting and Internalization of Ab-TC-Ln. Having proven the extracellular function of Ab-TC-Ln (LTX-VC-Ibt-DOTA-Eu, abbreviated to LTX-TC-Eu), we further investigated the cell targeting ability and internalization of Ab-TC-Ln toward Ramos cells. Initially, to evaluate their cell targeting and internalization ability through confocal immunofluorescence imaging, we labeled Ab-TC-Ln with FITC to prepare LTX/RTX-TC-Eu-FITC. As shown in Figure 5A, after incubation with LTX-TC-Eu-FITC for 2 h, green fluorescence emitted from FITC was observed on the cell membrane, indicating the binding of LTX-TC-Eu-FITC to CD19 on the Ramos cell surface. Notably, after incubation for 4 h, the LTX-TC-Eu-FITC-treated cells exhibited evident green fluorescence in the cytoplasm, demonstrating their uptake by Ramos cells. In contrast, we found that HepG2 cells (CD19-, CD20-) incubated with LTX-TC-Eu-FITC for 4 h did not exhibit fluorescence in the green channel (Figure S15). These results indicated that LTX-TC-Eu has the ability to target B-cell lymphoma cells (CD19+). The fluorescence of Ramos cells treated with RTX-TC-Eu-FITC for 16 h still showed on the cell membrane, not in the cytoplasm, indicating that RTX-TC-Eu-FITC cannot be internalized through CD20 into Ramos cells. We further detected the content of Eu at different times (0.5, 1, 2, 3, 4, 8, and 16 h) through ICP-MS to quantify the amount of LTX-TC-Eu internalized by cells over time (Figure S16). The uptake of LTX-TC-Eu by Ramos cells was found to be increased gradually at the beginning and reached a plateau after 4 h. On the contrary, the uptake of LTX-TC-Eu by HepG2 cells was negligible. These results indicated that LTX-TC-Eu had the ability to target B-cell lymphoma cells (CD19+) and could be internalized efficiently. These results suggest that LTX-TC-Eu can specifically bind to CD19 and be internalized by Ramos cells.

In Situ Reactivity and Selectivity of Ab-TC-Ln toward **BTK.** We further evaluated the in situ reactivity of LTX-TC-Eu in Ramos cells. Cell viability assays demonstrated that the cells incubated with 2 µM LTX-TC-Eu for 24 h exhibited no significant cytotoxicity (Figure S17). To demonstrate that the internalized LTX-TC-Eu can be cleaved by cathepsin B and the released Ibt-DOTA-Eu (TC-Eu) targeted covalently binds to cellular BTK, a competitive binding assay was applied using PCI-33380 (an irreversible fluorescence probe of BTK). PCI-33380 was found to form stable adducts with cellular BTK after 1 h of incubation (DMSO lane, PCI-33380-labeled BTK, Figure 5B). Pretreatment of Ramos cells with increasing concentration of LTX-TC-Eu gradually reduced the signal of the PCI-33380-labeled BTK band, and the BTK band was fully competed by 500 nM LTX-TC-Eu (Figure 5B). In contrast, RTX-TC-Eu was not able to eliminate the PCI-33380-BTK band even when its concentration reached 500 nM, consistent with the result that RTX-TC-Eu cannot penetrate Ramos cell membrane and release TC-Eu into the cytoplasm (Figure 5A). Pretreatment with 500 nM Ibt-DOTA-Eu had no influence on the PCI-33380-BTK band, which is attributed to the inability of Ibt-DOTA-Eu to penetrate the cell membrane.¹¹

To further investigate the in situ selectivity of LTX-TC-Eu, we evaluated its effect on the BTK-mediated BCR signaling pathway in Ramos cells through SDS-PAGE immunoblotting. We used anti-IgM, a mimic of BCR-antigen, to stimulate the

phosphorylation of BTK and its upstream (Syk) and downstream (PLCγ2, Erk1/2) kinases. As shown in Figure 5C, LTX-TC-Eu was observed to inhibit the phosphorylation of BTK as well as its downstream kinases (PLCγ2, Erk1/2) in a concentration-dependent manner, and 100 nM LTX-TC-Eu was found to significantly inhibit the phosphorylation of these kinases. The phosphorylation of the upstream kinase Syk was not affected, suggesting that BTK is the specific target of the released TC-Eu. LTX alone cannot affect BCR signaling even when its concentration reaches 500 nM, which implies the indispensable role of TC-Eu in the inhibition of the BCR signaling pathway. As shown in Figure S18, following pretreatment with the cathepsin B inhibitor CA-074ME (10 μ M), Ibt-DOTA-Eu cannot be released from LTX-TC-Eu and inhibit BTK phosphorylation in Ramos cells. These results demonstrate that LTX-TC-Eu can be specifically internalized and cleaved by cellular cathepsin B, and the released TC-Eu efficiently inhibits cellular BTK and the BCR signaling pathway.

Quantification of Cellular BTK with LTX-TC-Eu through HPLC/SUID-ICP-MS. Having proven the in situ function of LTX-TC-Eu in Ramos cells, we further explored its ability to quantify cellular BTK by using the HPLC/SUID-ICP-MS technology. As shown in Figure 5D,1, the peaks in the SEC-UV chromatogram show poor resolution, which indicates the complexity of cell lysates. In contrast, clear peaks corresponding to BTK-TC-Eu were found in 151Eu/153Eu isotope chromatograms (Figure 5D,2), indicating the excellent anti-interference ability of ICP-MS for real sample analysis. BTK is the only protein found labeled by TC-Eu and detected by ICP-MS (25.1 min), further demonstrating the high selectivity of the released TC-Eu to active BTK in Ramos cells. To obtain the accurate BTK quantification result, the online-measured 151Eu/153Eu isotope chromatograms were transformed into Eu mass flow chromatogram (Figure 5D,3), and the concentration of active BTK in Ramos cells was determined to be $108.7 \pm 7.2 \text{ ng/1} \times 10^6 \text{ cells (mean } \pm \text{ s.d., } n$ = 3) consistent with the previous results. 11 The result of Western blot analysis in Figure S19 revealed a BTK expression level in Ramos cells of 128.1 \pm 19.1 ng/10⁶ cells (mean \pm s.d., n = 3), which is higher than the result obtained by our method. The proposed reason is that the BTK determined by our method is the active form, a portion of the total BTK (i.e., including both active and inactive forms) determined by Western blot analysis. The same method was applied to OCI-LY10 cells (diffuse large B-cell lymphoma cells, CD19+), of which the BTK concentration was determined to be 132.7 \pm 11.7 ng/10⁶ cells (Figure S20). To the best of our knowledge, this is the first study to realize the active BTK quantification in live cells through using the strategy of antibody-directed cell internalization of a targeted covalent lanthanide tag.

CONCLUSIONS

We have established a novel antibody-directed cells and proteins dual-targeting strategy for in situ labeling and quantifying protein targets involving a multifunctional **Ab-TC-Ln**. This study addresses the challenge of the lack of cell targeting property and low cellular uptake as a result of the inability to penetrate the cell membrane of the DOTA-based TC-Ln for in situ protein target labeling. Benefiting from the high reactivity and selectivity of TC-Ln, we achieve accurate quantitation of active BTK within B-cell lymphoma cells by using HPLC/SUID-ICP-MS. We believe that the promising

strategy established in this study will inspire the development of new ICP-MS approaches toward the quantification of other important protein targets in the future. Furthermore, new targeted radionuclide drugs could be developed by replacing the natural Ln ion in **Ab-TC-Ln** with radionuclide for theranostics of different cancers in the future.²⁵

ASSOCIATED CONTENT

Supporting Information

The Supporting Information is available free of charge at https://pubs.acs.org/doi/10.1021/acs.analchem.5c00508.

General considerations and experimental procedures and additional figures and tables; ESI-MS spectrum of compound c (Figure S1); ESI-MS spectrum of compound e (Figure S2); ESI-MS spectrum of compound h (Figure S4); HPLC-ESI-MS analysis of LTX reduced by TCEP (Figure S8); mass spectra of LTX-/RTX-Ibt-Eu as determined by MALDI-ToF MS (Figure S12); confocal fluorescence image of HepG2 cells (CD19–, CD20–) stained by Ab-TC-FITC (2 μ M) (Figure S15); (A) 151 Eu and 153 Eu signal intensity of BTK labeled by LTX-TC-Eu in OCI-LY10 cells characterization by SEC-ICP-MS. (B) Eu mass flow chromatogram of the Eu-labeled BTK transformed from (A) (Figure S20) (PDF)

AUTHOR INFORMATION

Corresponding Author

Xiaowen Yan — Department of Chemistry and the MOE Key Laboratory of Spectrochemical Analysis & Instrumentation, College of Chemistry and Chemical Engineering, Xiamen University, Xiamen 361005, China; Innovation Laboratory for Sciences and Technologies of Energy Materials of Fujian Province (IKKEM), Xiamen 361005, China; orcid.org/0000-0001-6608-6044; Email: xwyan@xmu.edu.cn

Authors

Ziyang Fang — Department of Chemistry and the MOE Key Laboratory of Spectrochemical Analysis & Instrumentation, College of Chemistry and Chemical Engineering, Xiamen University, Xiamen 361005, China

Xinyue Zhao — Department of Chemistry and the MOE Key Laboratory of Spectrochemical Analysis & Instrumentation, College of Chemistry and Chemical Engineering, Xiamen University, Xiamen 361005, China

Ruxue Hou – Department of Chemistry and the MOE Key Laboratory of Spectrochemical Analysis & Instrumentation, College of Chemistry and Chemical Engineering, Xiamen University, Xiamen 361005, China

Yang Zhao – Department of Chemistry and the MOE Key Laboratory of Spectrochemical Analysis & Instrumentation, College of Chemistry and Chemical Engineering, Xiamen University, Xiamen 361005, China

Lei Wang – Department of Chemistry and the MOE Key Laboratory of Spectrochemical Analysis & Instrumentation, College of Chemistry and Chemical Engineering, Xiamen University, Xiamen 361005, China

Li Yi – Department of Chemistry and the MOE Key Laboratory of Spectrochemical Analysis & Instrumentation, College of Chemistry and Chemical Engineering, Xiamen University, Xiamen 361005, China

Limin Yang — Department of Chemistry and the MOE Key Laboratory of Spectrochemical Analysis & Instrumentation, College of Chemistry and Chemical Engineering, Xiamen University, Xiamen 361005, China

Qiuquan Wang — Department of Chemistry and the MOE Key Laboratory of Spectrochemical Analysis & Instrumentation, College of Chemistry and Chemical Engineering, Xiamen University, Xiamen 361005, China; orcid.org/0000-0002-5166-4048

Complete contact information is available at: https://pubs.acs.org/10.1021/acs.analchem.5c00508

Author Contributions

[§]Z.F., X.Z., and R.H. contributed equally to this work.

The authors declare no competing financial interest.

ACKNOWLEDGMENTS

This study was financially supported by the National Key Research and Development Program of China (2022YFF0710200), the National Natural Science Foundation of China (22074127 and 22193053), the Science and Technology Projects of Innovation Laboratory for Sciences and Technologies of Energy Materials of Fujian Province (IKKEM) (HRTP-[2022]-13), and the Fundamental Research Funds for the Central Universities (20720200073).

REFERENCES

- (1) Zhang, C.; Wu, F.; Zhang, Y.; Wang, X.; Zhang, X. J. Anal. At. Spectrom. 2001, 16, 1393–1396.
- (2) Arnett, L. P.; Rana, R.; Chung, W. W.-Y.; Li, X.; Abtahi, M.; Majonis, D.; Bassan, J.; Nitz, M.; Winnik, M. A. Chem. Rev. 2023, 123, 1166–1205.
- (3) Yan, X.; Luo, Y.; Zhang, Z.; Li, Z.; Luo, Q.; Yang, L.; Zhang, B.; Chen, H.; Bai, P.; Wang, Q. Angew. Chem., Int. Ed. 2012, 51, 3358–3363
- (4) Yin, X.; Yang, B.; Chen, B.; He, M.; Hu, B. Anal. Chem. 2019, 91, 10596–10603.
- (5) Han, G.; Spitzer, M. H.; Bendall, S. C.; Fantl, W. J.; Nolan, G. P. *Nat. Protoc.* **2018**, *13*, 2121–2148.
- (6) Bendall, S. C.; Simonds, E. F.; Qiu, P.; Amir, E.-a. D.; Krutzik, P. O.; Finck, R.; Bruggner, R. V.; Melamed, R.; Trejo, A.; Ornatsky, O. I.; Balderas, R. S.; Plevritis, S. K.; Sachs, K.; Pe'er, D.; Tanner, S. D.; Nolan, G. P. *Science* **2011**, 332, 687–696.
- (7) Zhang, C.; Wu, F.; Zhang, X. J. Anal. At. Spectrom. 2002, 17, 1304–1307.
- (8) Hu, S.; Zhang, S.; Hu, Z.; Xing, Z.; Zhang, X. Anal. Chem. 2007, 79, 923–929
- (9) Ornatsky, O. I.; Lou, X.; Nitz, M.; Schäffer, S.; Sheldrick, W. S.; Baranov, V. I.; Bandura, D. R.; Tanner, S. D. *Anal. Chem.* **2008**, *80*, 2539–2547.
- (10) Terenghi, M.; Elviri, L.; Careri, M.; Mangia, A.; Lobinski, R. *Anal. Chem.* **2009**, *81*, 9440–9448.
- (11) Yan, X.; Gu, Y.; Zhao, Y.; Zhao, X.; Yang, L.; Yan, X.; Wang, Q. At. Spectrosc. **2024**, 45, 74–82.
- (12) Han, G.; Zhang, S.; Xing, Z.; Zhang, X. Angew. Chem., Int. Ed. 2013, 52, 1466-1471.
- (13) Yan, X.; Xu, M.; Yang, L.; Wang, Q. Anal. Chem. 2010, 82, 1261-1269.
- (14) Lou, X.; Zhang, G.; Herrera, I.; Kinach, R.; Ornatsky, O.; Baranov, V.; Nitz, M.; Winnik, M. A. Angew. Chem., Int. Ed. 2007, 46, 6111–6114
- (15) Zhao, Y.; Zhao, X.; Duan, L.; Hou, R.; Gu, Y.; Liu, Z.; Chen, J.; Wu, F.; Yang, L.; Le, X. C.; Wang, Q.; Yan, X. J. Med. Chem. **2024**, *67*, 5458–5472.

- (16) Ji, C.; Liang, Y.; Ge, F.; Yang, L.; Wang, Q. Anal. Chem. 2019, 91, 7032–7038.
- (17) Liu, R.; Hou, X.; Lv, Y.; McCooeye, M.; Yang, L.; Mester, Z. Anal. Chem. **2013**, *85*, 4087–4093.
- (18) Gómez-Espina, J.; Blanco-González, E.; Montes-Bayón, M.; Sanz-Medel, A. J. Anal. At. Spectrom. 2016, 31, 1895–1903.
- (19) Aoki, Y.; Isselbacher, K. J.; Pillai, S. Proc. Natl. Acad. Sci. U.S.A. 1994, 91, 10606–10609.
- (20) Satterthwaite, A. B.; Cheroutre, H.; Khan, W. N.; Sideras, P.; Witte, O. N. Proc. Natl. Acad. Sci. U.S.A. 1997, 94, 13152–13157.
- (21) Pan, Z.; Scheerens, H.; Li, S.-J.; Schultz, B. E.; Sprengeler, P. A.; Burrill, L. C.; Mendonca, R. V.; Sweeney, M. D.; Scott, K. C. K.; Grothaus, P. G.; Jeffery, D. A.; Spoerke, J. M.; Honigberg, L. A.; Young, P. R.; Dalrymple, S. A.; Palmer, J. T. *ChemMedChem* **2007**, *2*, 58–61.
- (22) Lee, A. Drugs 2021, 81, 1229-1233.
- (23) Rougé, L.; Chiang, N.; Steffek, M.; Kugel, C.; Croll, T. I.; Tam, C.; Estevez, A.; Arthur, C. P.; Koth, C. M.; Ciferri, C.; Kraft, E.; Payandeh, J.; Nakamura, G.; Koerber, J. T.; Rohou, A. *Science* **2020**, 367, 1224–1230.
- (24) Doronina, S. O.; Bovee, T. D.; Meyer, D. W.; Miyamoto, J. B.; Anderson, M. E.; Morris-Tilden, C. A.; Senter, P. D. *Bioconjugate Chem.* **2008**, *19*, 1960–1963.
- (25) Cui, X.-Y.; Li, Z.; Kong, Z.; Liu, Y.; Meng, H.; Wen, Z.; Wang, C.; Chen, J.; Xu, M.; Li, Y.; Gao, J.; Zhu, W.; Hao, Z.; Huo, L.; Liu, S.; Yang, Z.; Liu, Z. *Nature* **2024**, *630*, 206–213.



CAS BIOFINDER DISCOVERY PLATFORM™

CAS BIOFINDER HELPS YOU FIND YOUR NEXT BREAKTHROUGH FASTER

Navigate pathways, targets, and diseases with precision

Explore CAS BioFinder

